Electronic supplementary information (ESI)

Stabilization of planar tetracoordinate silicon in the 2D-layered extended system and design of high-capacity anode material for Li-ion batteries

Ming-Jun Sun,[†] Xinrui Cao,[*,‡] and Zexing Cao [*,†]

[†] State Key Laboratory of Physical Chemistry of Solid Surfaces and Department of Chemistry, College of Chemistry and Chemical Engineering, Xiamen University, Xiamen 361005, China.

[‡] Department of Physics and Collaborative Innovation Center for Optoelectronic Semiconductors and Efficient Devices, Fujian Provincial Key Laboratory of Theoretical and Computational Chemistry, Xiamen University, Xiamen 361005, China.

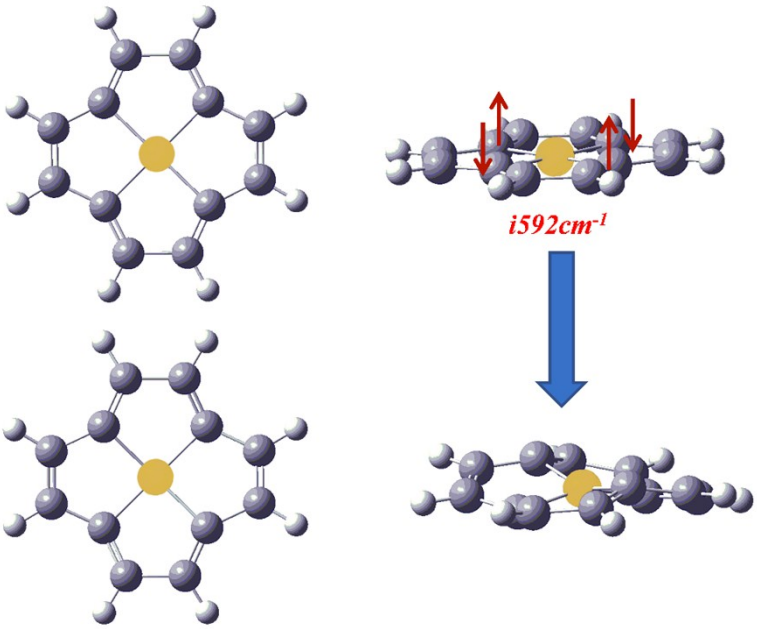

Fig. S1 The optimized structures of ptSi-$C_{12}H_8Si$ and ttSi-$C_{12}H_8Si$ molecules, as well as the vibrational mode with an imaginary frequency of the ptSi-$C_{12}H_8Si$ molecule.

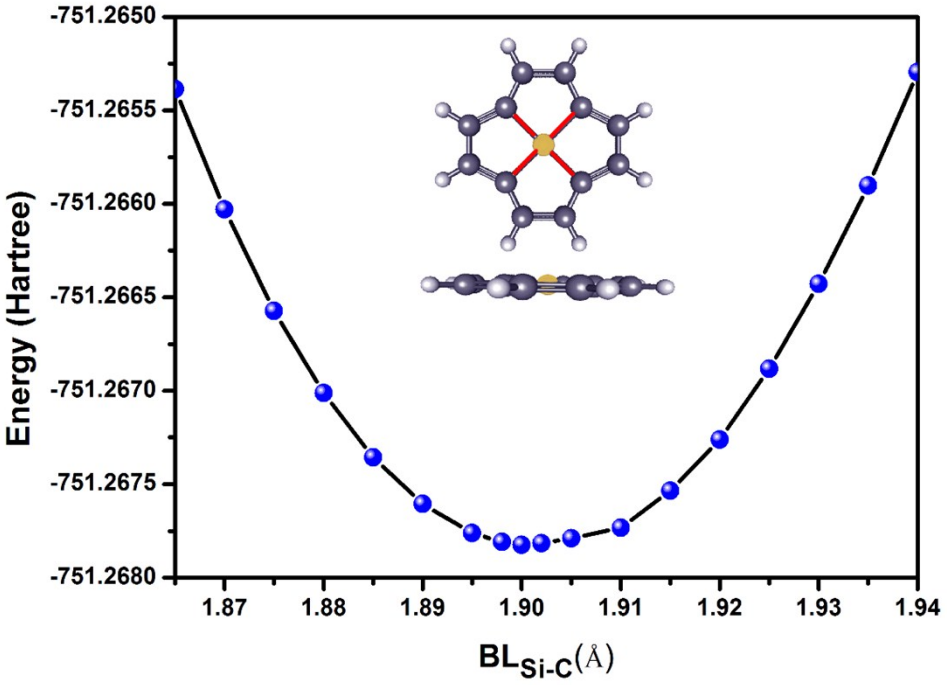

Fig. S2 The energy curve of ptSi-$C_{12}H_8Si$ molecule as a function of the Si-C distance.

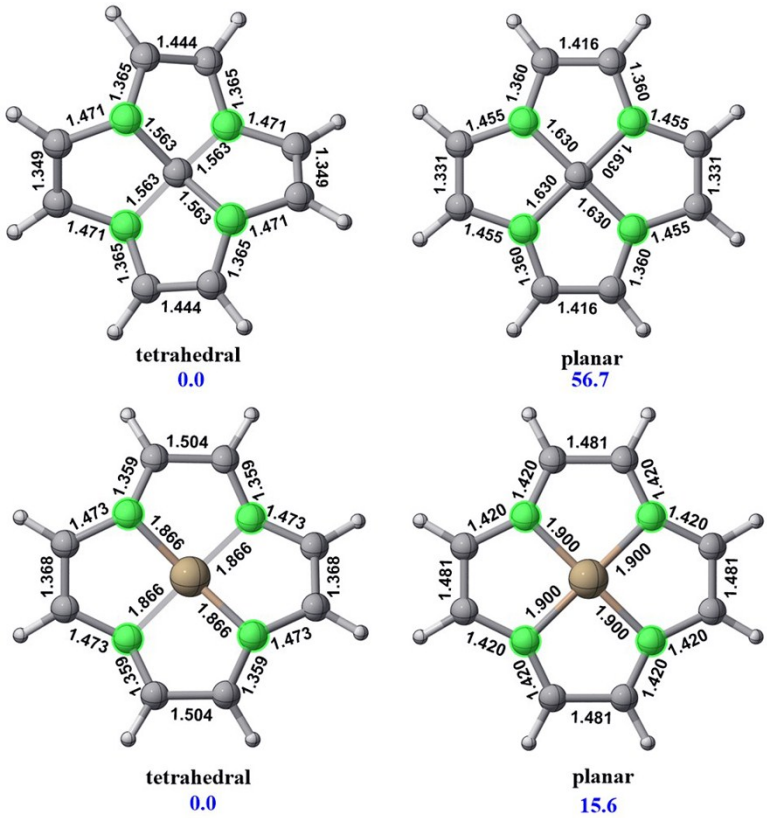

Fig. S3 The energy differences between the planar and twisted tetracoordinate structures for $C_{13}H_8$ and $C_{12}H_8Si$ molecules, in which the green color just refers to the carbon atoms linking to the silicon atom.

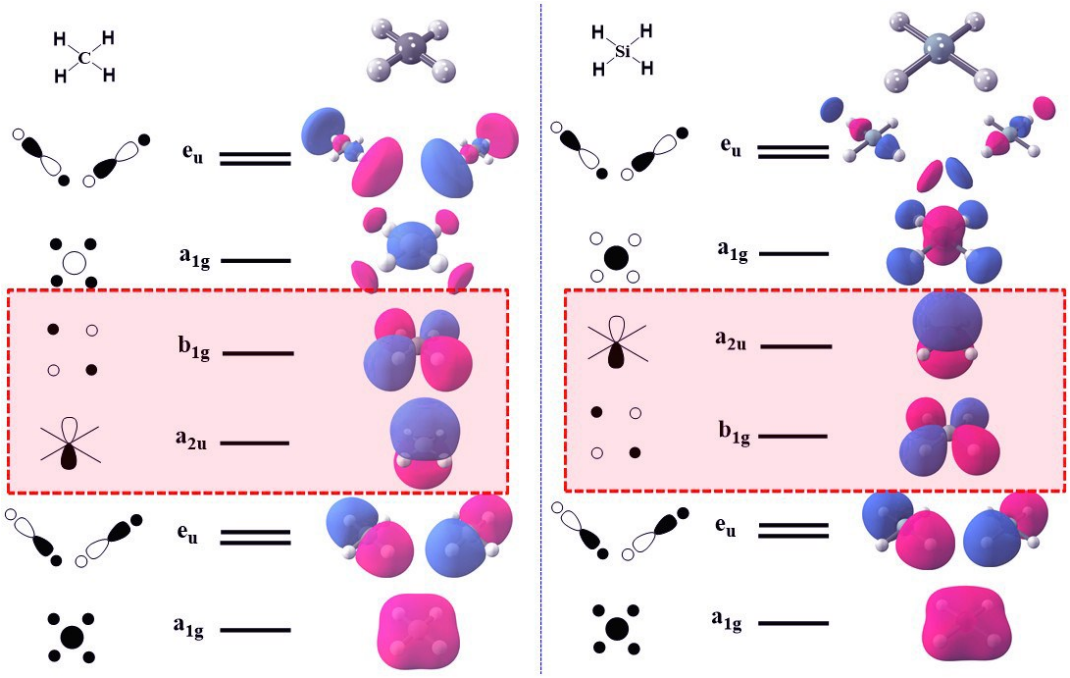

Fig. S4 Walsh diagrams for selected frontier molecular orbitals of square planar CH_4 and SiH_4 molecules.

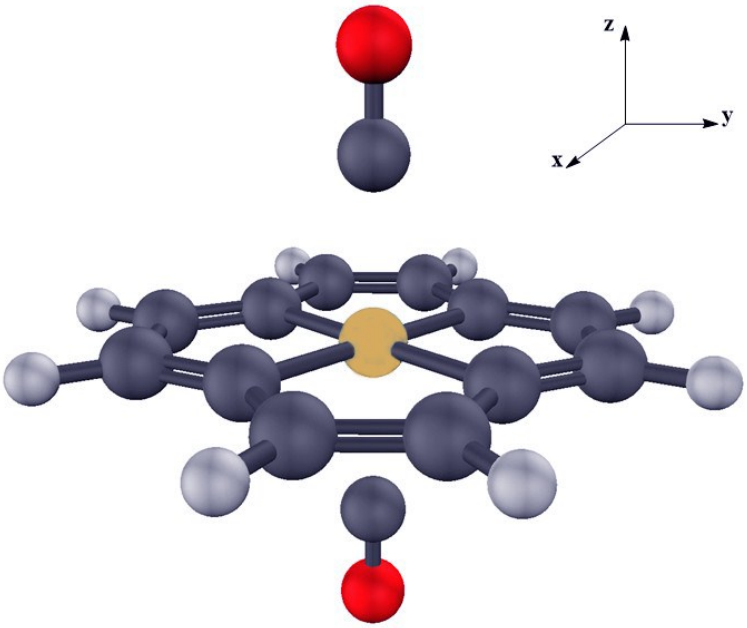

Fig. S5 The interactions between $C_{12}H_8Si$ molecule and two CO molecules.

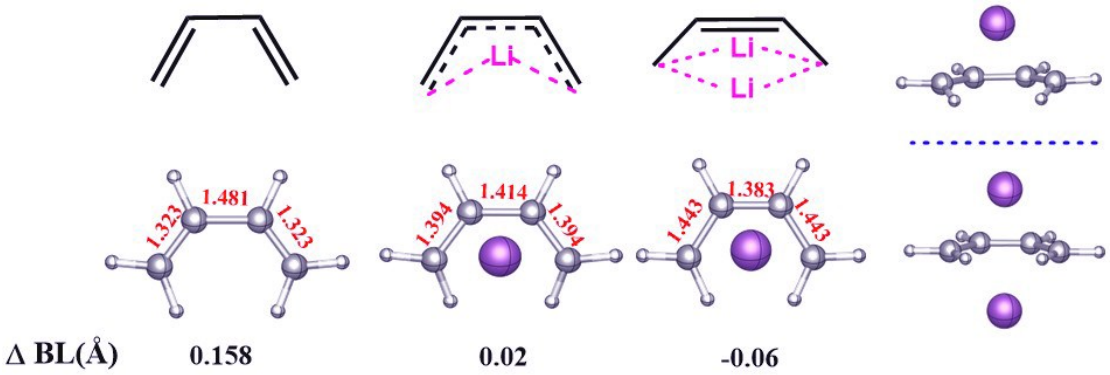

Fig. S6 The interactions between 1,3-butadiene and lithium atoms and the optimized structures of their complexes.

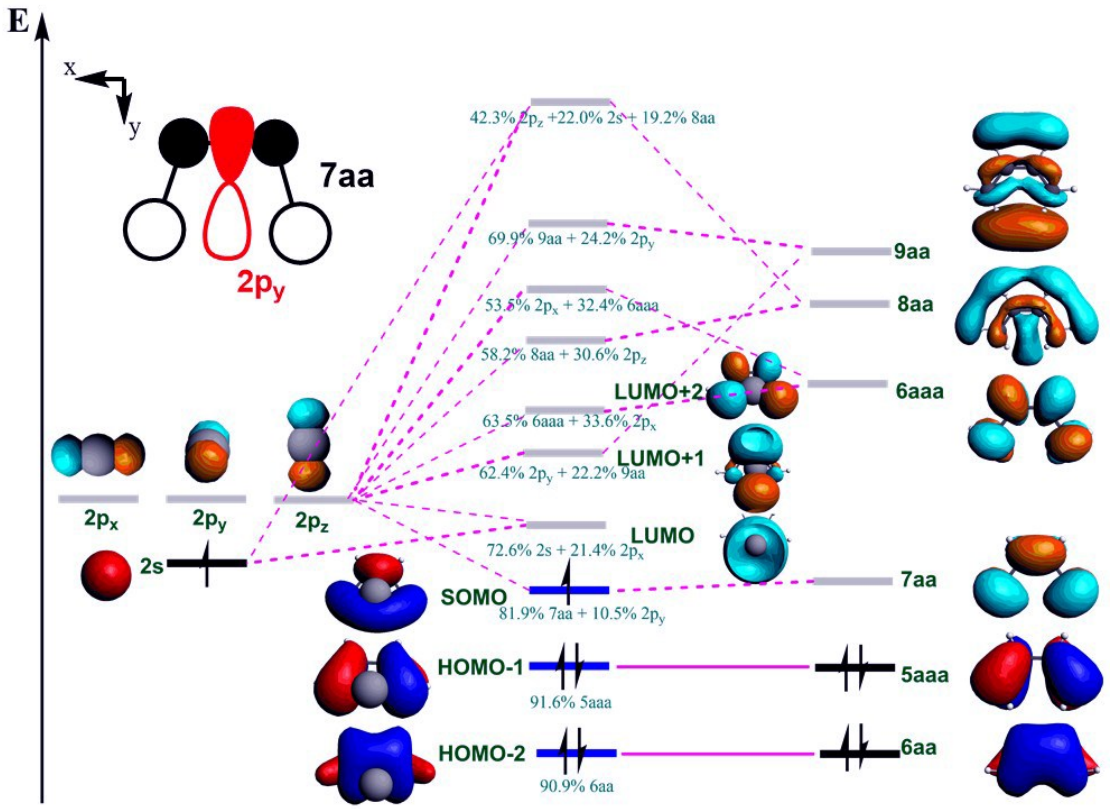

Fig. S7 The orbital interactions between 1,3-butadiene and lithium atom.

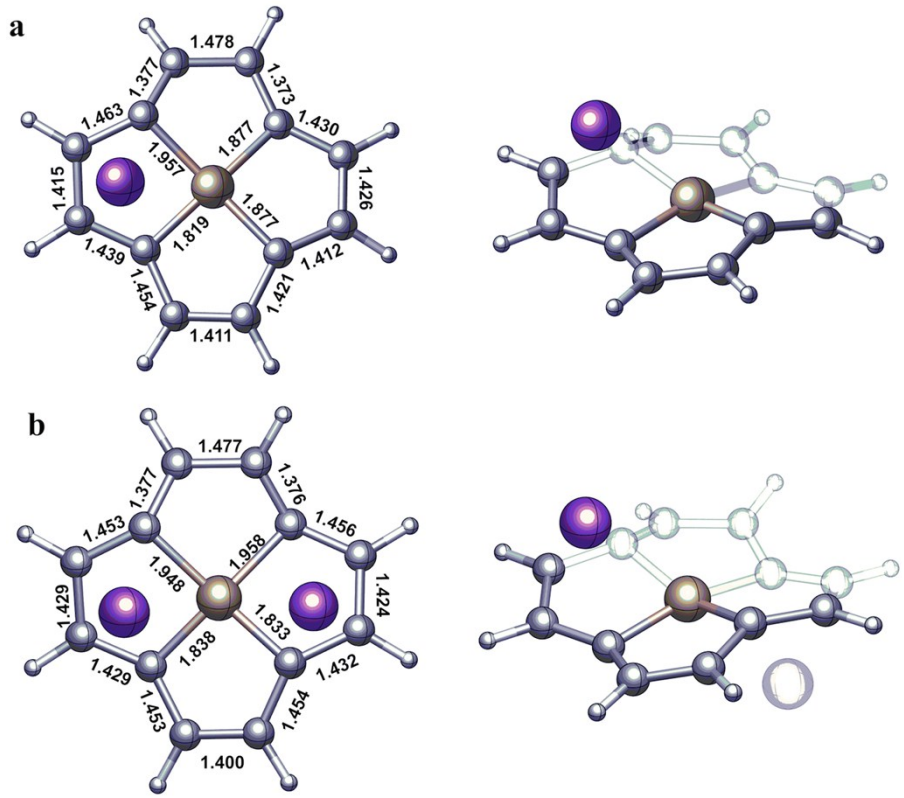

Fig. S8 The interactions between the $C_{12}H_8Si$ molecule and lithium. (**a**) Li. (**b**). 2Li

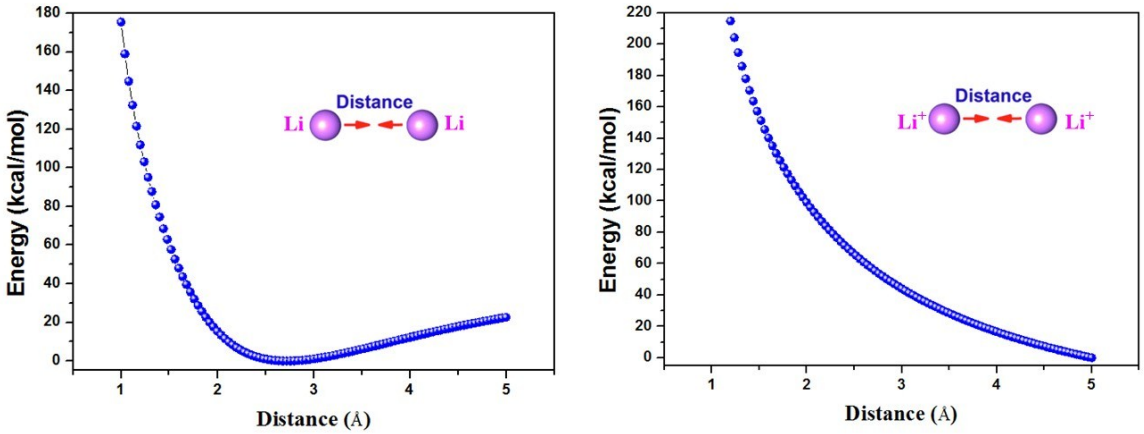

Fig. S9 The relative energy profiles of Li_2 and Li_2^{2+} as a function of the Li-Li or the Li^+-Li^+ distance, respectively.

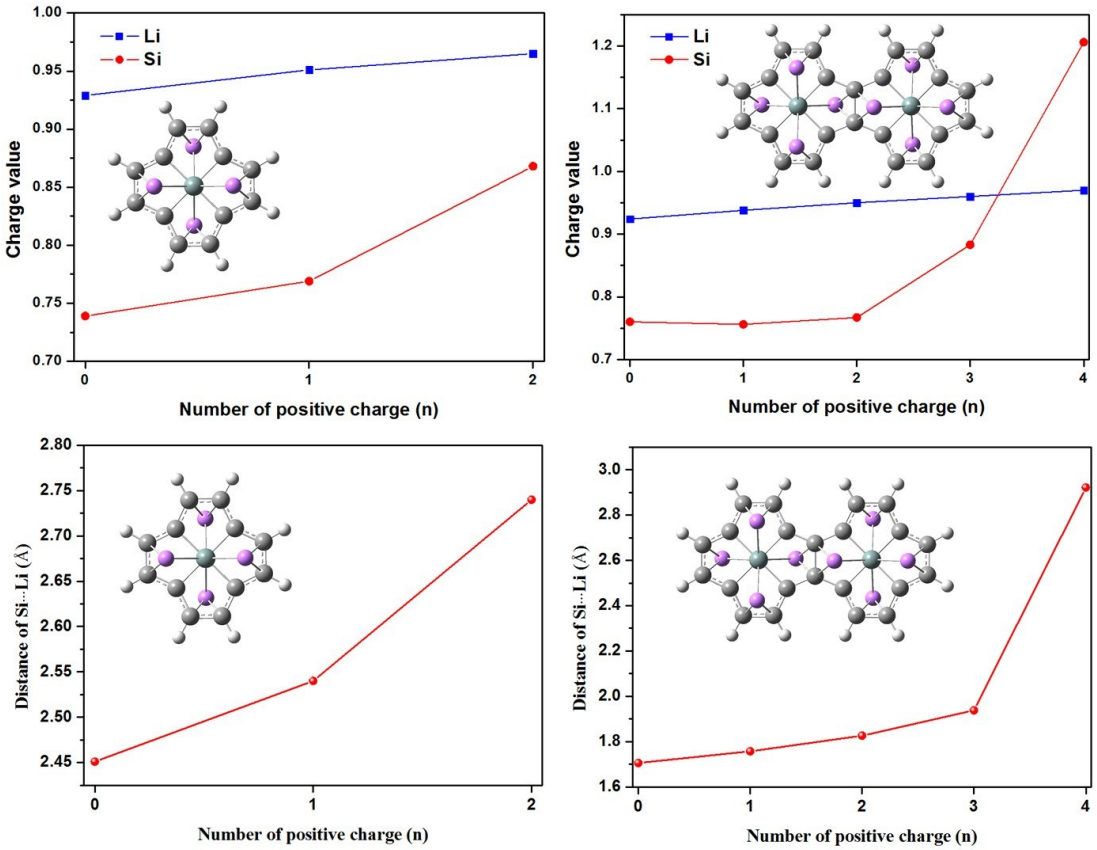

Fig. 10. Selected NBO charges and distances of Si···Li as the function of different positive charges in the $SiC_{12}H_8Li_4$ and $Si_2C_{22}H_{12}Li_8$ complexes.

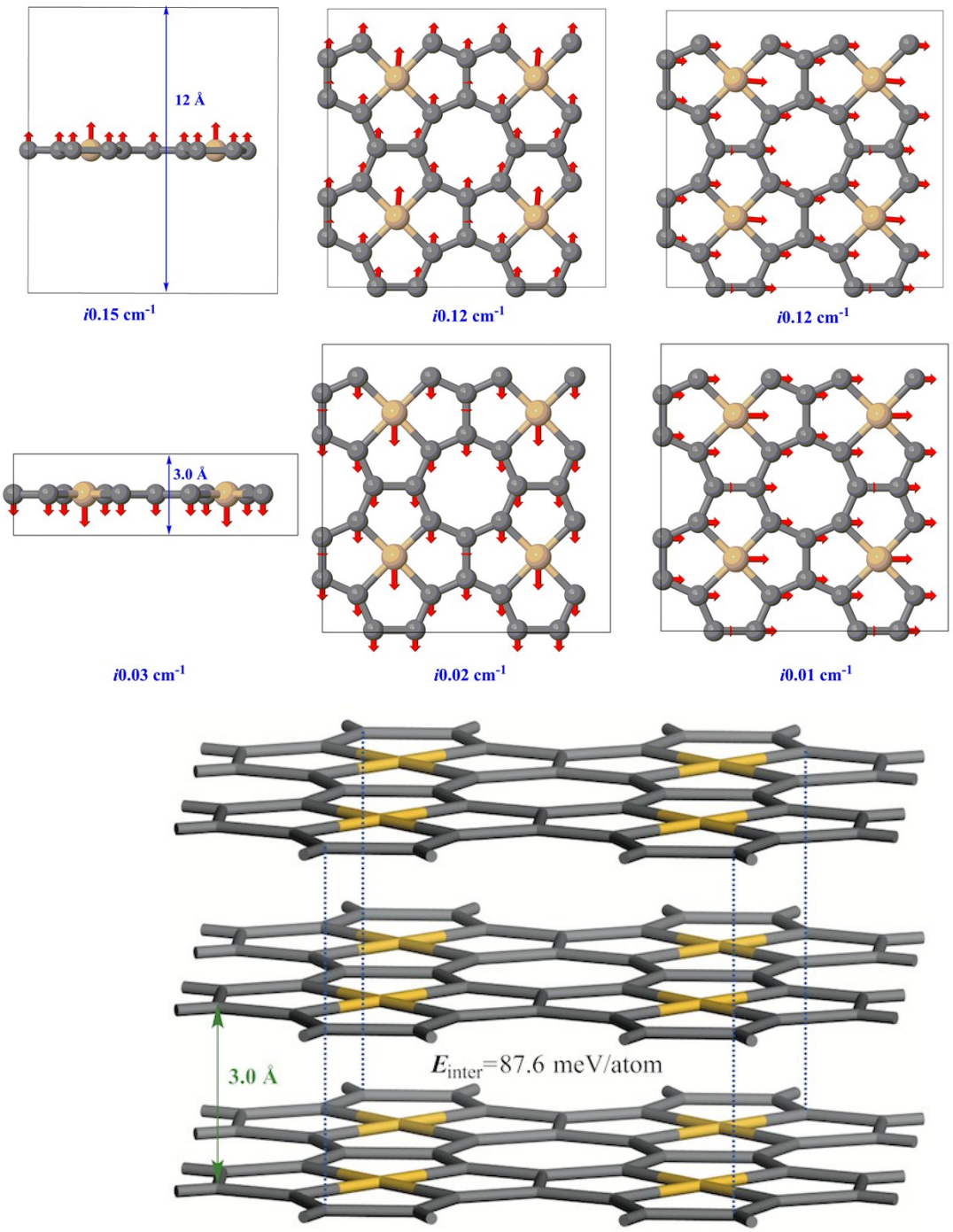

Fig. S11 The translational modes with imaginary frequencies for the monolayer SiC_8 siligraphene (top) and the SiC_8 siligraphite (middle), as well as the optimized structure of the SiC_8 siligraphite (bottom).

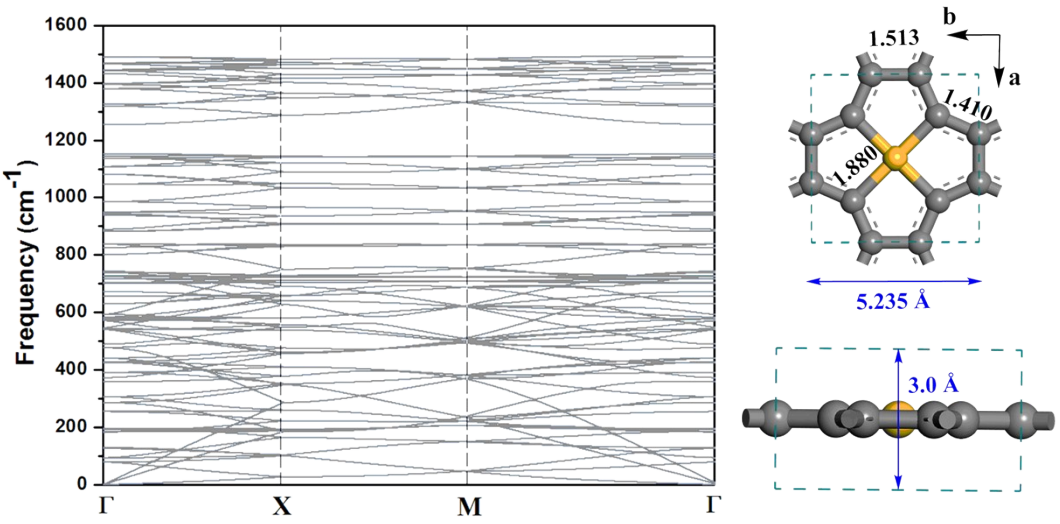

Fig. S12 Phonon dispersion of the SiC_8 siligraphite with the layer-by-layer interaction. Γ(0,0,0), X(0.5,0,0), and M(0.5,0.5,0) refer to special points in the first Brillouin zone in the reciprocal space.

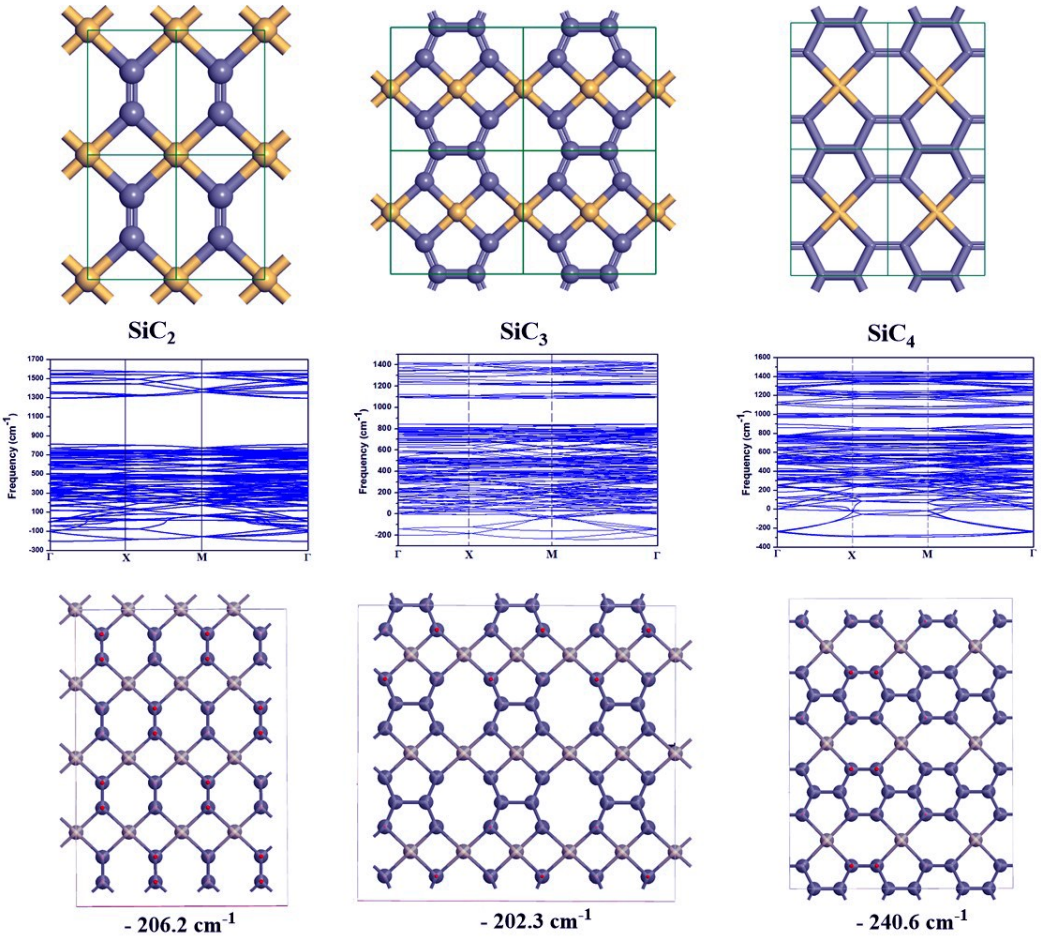

Fig. S13 Phonon spectra and the vibrational modes with the largest imaginary frequency for the SiC_2, SiC_3, and SiC_4 siligraphenes.

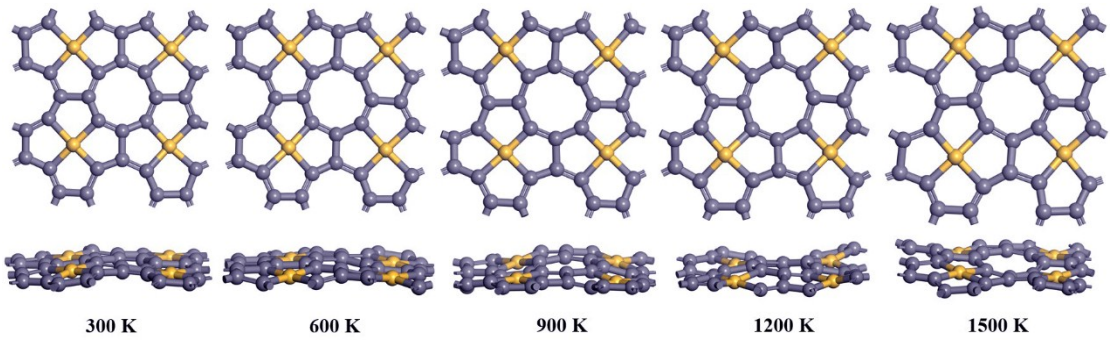

Fig. S14 Snapshots of the final frame from the 10 ps AIMD simulations at temperatures from 300 to 1500 K (top and side views). Bonds to atoms outside this 2 × 2 section are not shown here.

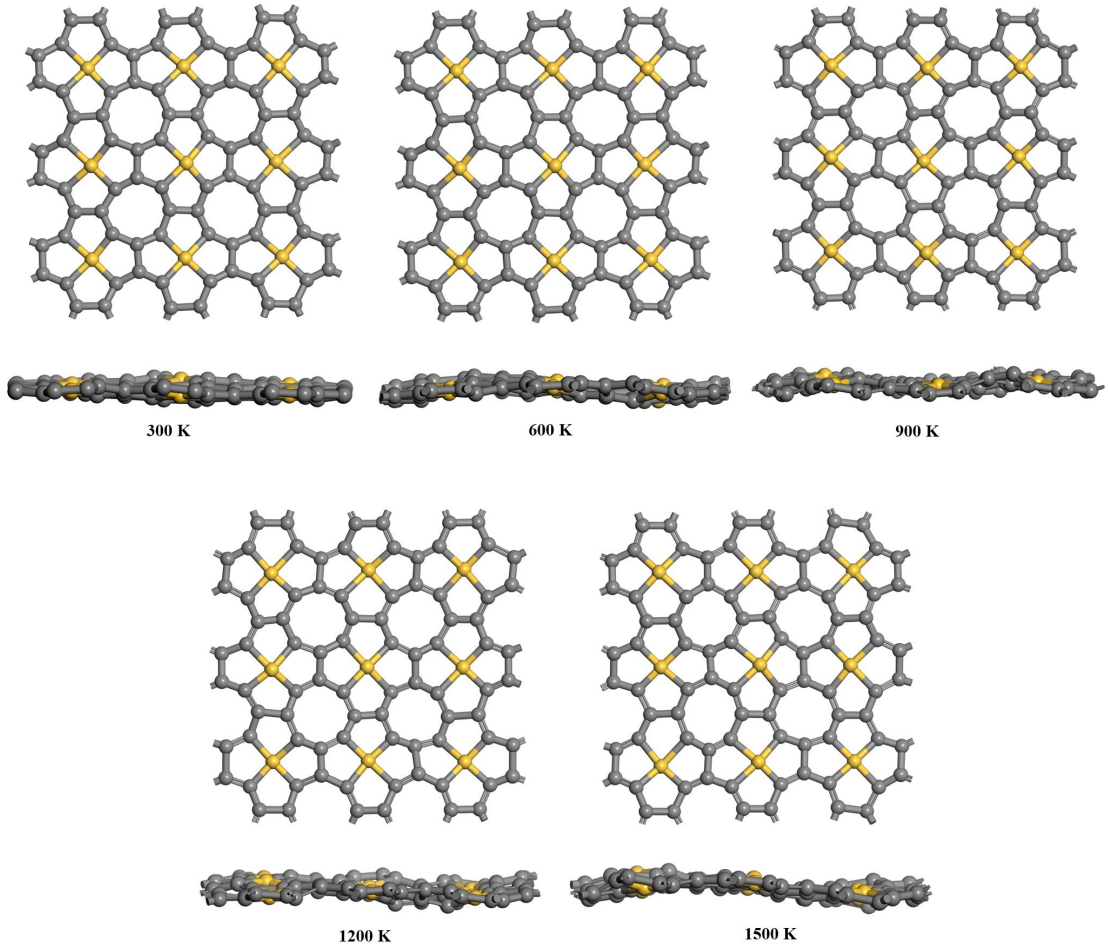

Fig. S15 Snapshots of the final frame from the 10 ps AIMD simulations at temperatures from 300 to 1500 K (top and side views). Bonds to atoms outside this 3 × 3 section are not shown here.

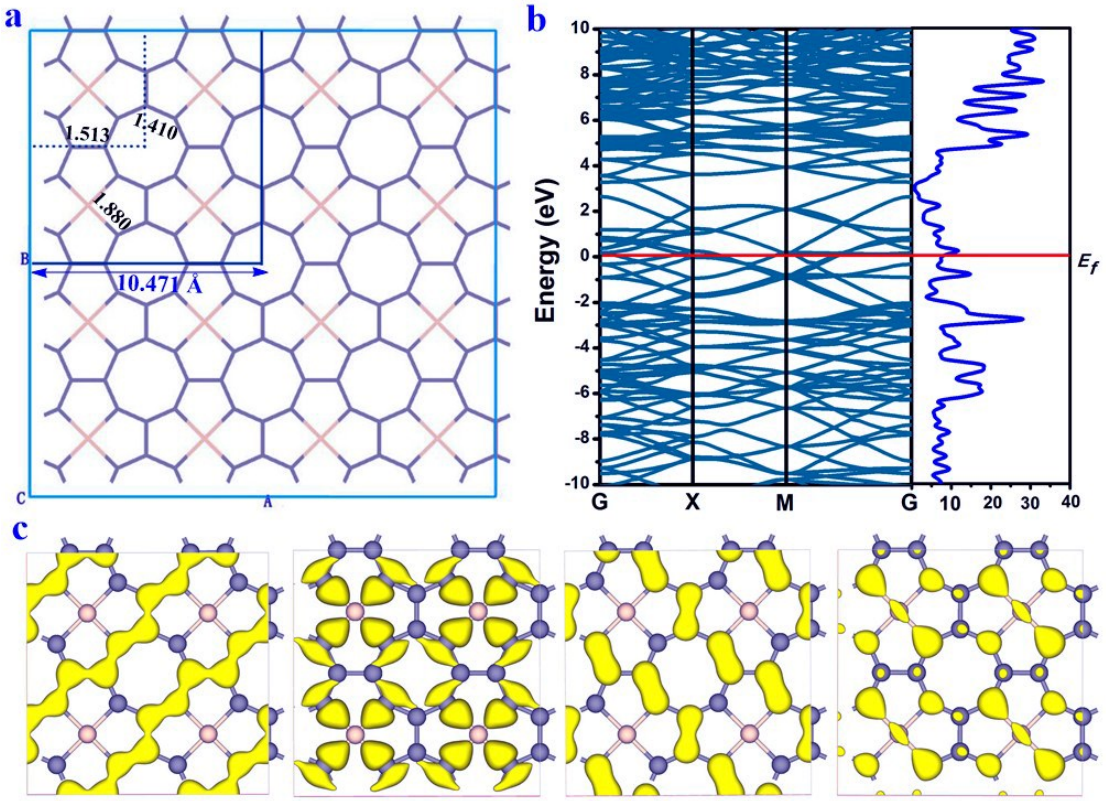

Fig. S16 (a) The 2×2 units of the SiC_8 siligraphene. (b) Electronic band structure (left) and total density of states (right) of the SiC_8 siligraphene. (c) The electronic states (HOES-1, HOES, HUES, HUES-1) of the SiC_8 siligraphene at the X point. The isosurface value is 0.4 e/au.

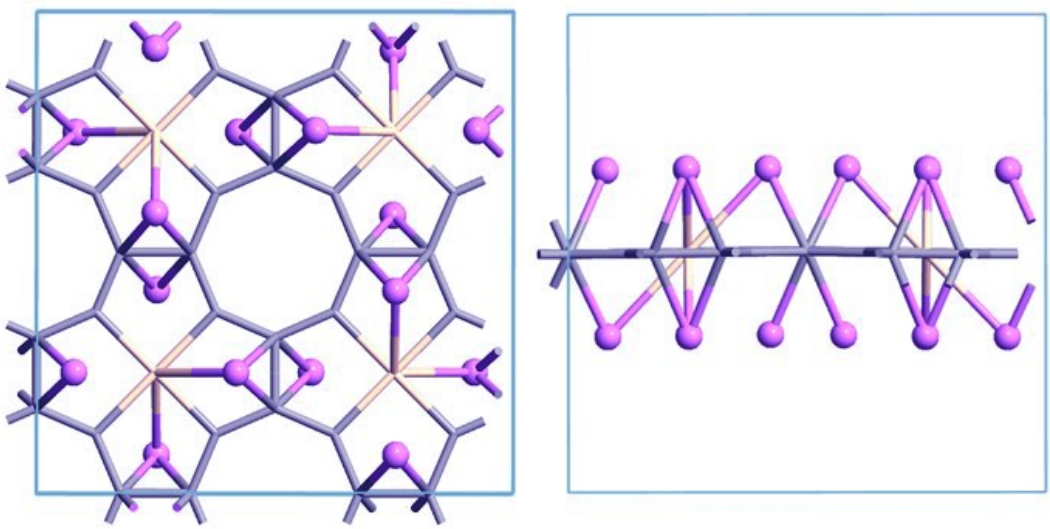

Fig. S17 The optimized 2D structure of the $Si_4C_{32}Li_{16}$ complex (Left for the top view and right for the side view).

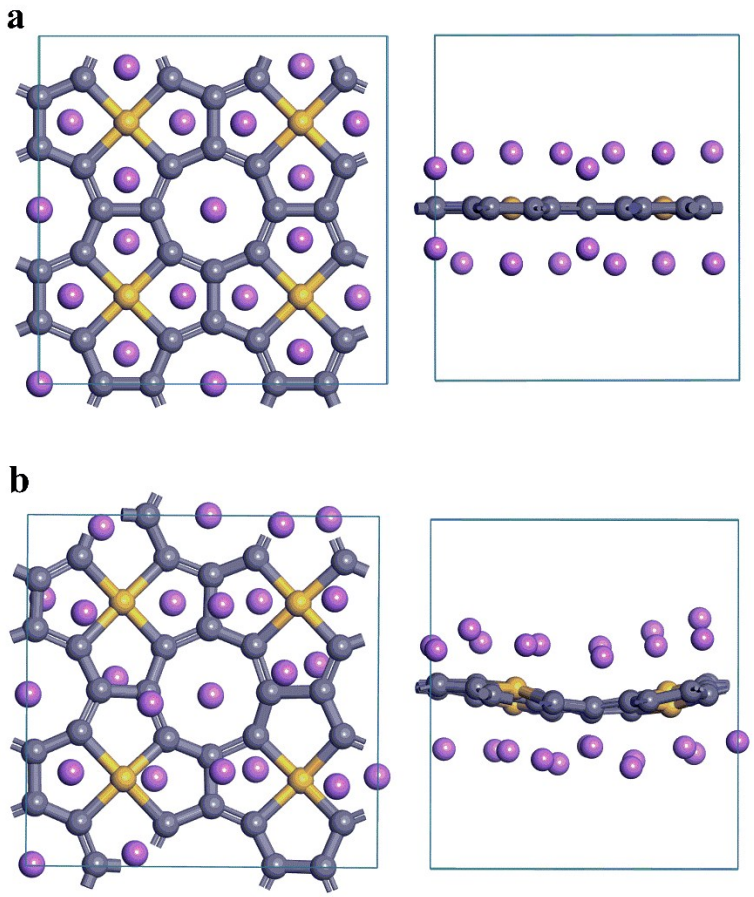

Fig. S18 **a.** The optimized 2D structure of the $Si_4C_{32}Li_{24}$ complex. **b.** The last snapshot from the 10 ps AIMD simulations at the temperature of 340 K.

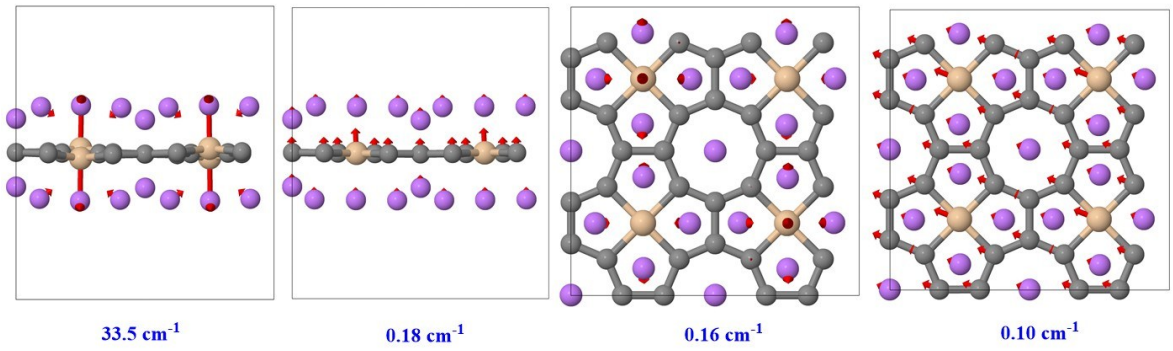

Fig. S19 The out-of-plane mode with an imaginary frequency and three transitional modes in the $Si_4C_{32}Li_{24}$ complex.

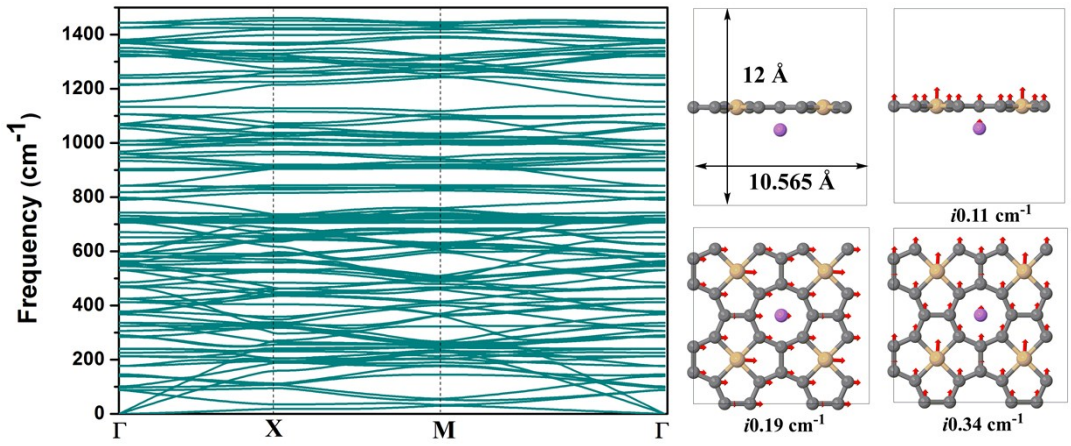

Fig. S20 Phonon spectrum and three transitional modes of the $Si_4C_{32}Li$ complex.

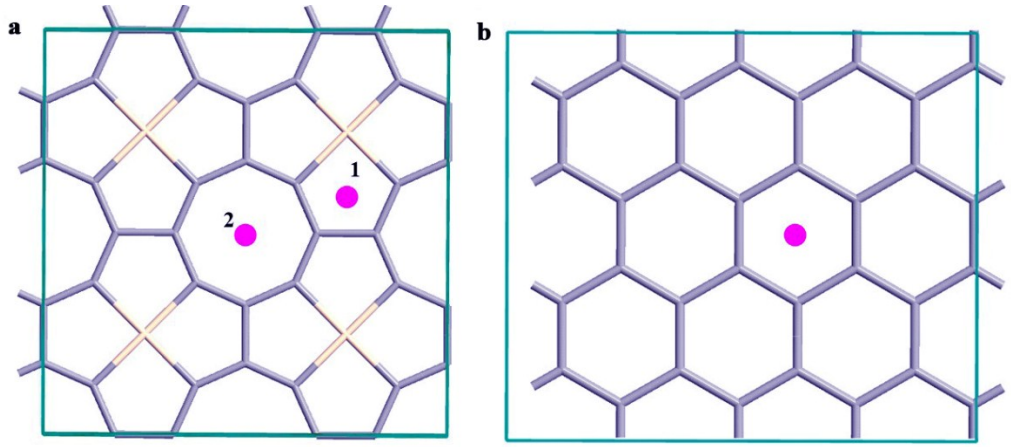

Fig. S21 a. The adsorption interaction between lithium and SiC_8 siligraphene at the most favorable sites **1** and **2**. **b**. The adsorption interaction between lithium and graphene.

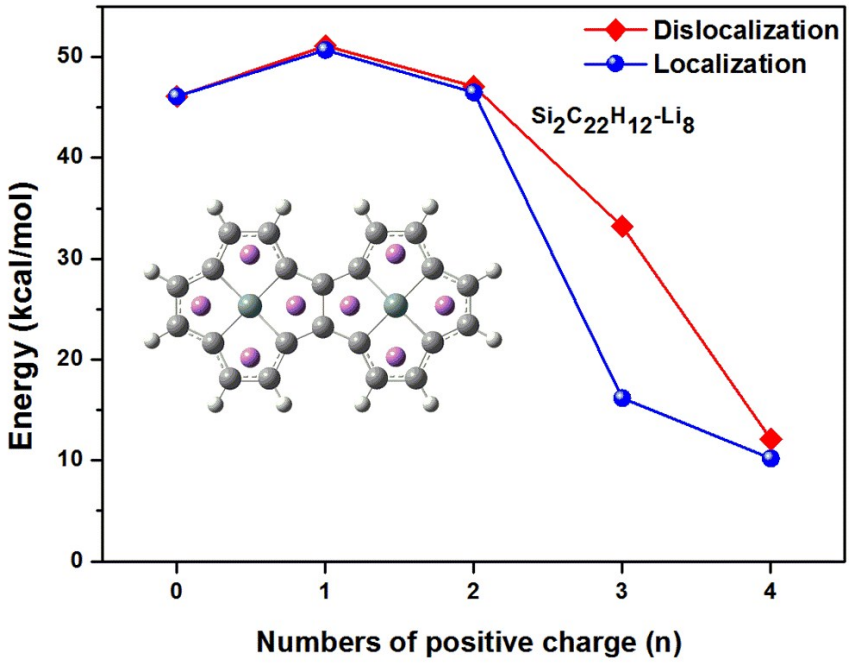

Fig. S22 The average adsorption energy of of lithium in $Si_2C_{22}H_{12}Li_8$ complex with different positive charges.

Table S1. The relative energies (kcal/mol) of complexes with different configurations and spin multiplicities.

$C_{12}H_8Si\text{-}Li_2$				
Spin multiplicity	**para-ud**	**para-uu**	**ortho-ud**	**ortho-uu**
S=1	0.0	0.6	2.1	4.9
S=3	10.3	10.2	8.1	11.1
$C_{12}H_8Si\text{-}Li_4$				
Spin multiplicity	**udud**		**uudd**	**uuuu**
S=1	0.0		7.4	9.5
S=3	29.2		33.6	35.4
S=5	73.2		71.5	80.3

Table S2. The interaction energies (kcal/mol) between lithium atom & ion with the C_4H_6 and C_6H_6 molecules.

Complexes	**Methods**			
	B3LYP/6-31G(d)	**M062X/6-31G(d)**	**HSEH1PBE/6-31G(d)**	**MP2/6-31G(d)**
C_4H_6-Li	25.0	28.7	26.9	14.9
C_4H_6-Li^+	32.9	32.6	32.8	32.7
C_6H_6-Li	3.7	7.4	5.3	6.3
C_6H_6-Li^+	40.6	41.2	41.0	41.7

Table S3. The calculated average interaction energies (kcal/mol) between lithium and the Si-C clusters and the aromatic system at the B3LYP/6-31G(d) level (The interaction energies for SiC_8 siligraphene and graphene are calculated by the GGA-PBE functional implemented in the VASP package).

Complexes	Lithium atom	Lithium ion
Silicon carbon clusters		
$SiC_{12}H_8$	37.7	42.5
$Si_2C_{22}H_{12}$	41.2	53.2
$Si_4C_{40}H_{16}$	54.4	**52.3 (1) / 60.0 (2)**
SiC_8 siligraphene	**48.8 (1) / 59.7 (2)**	
Aromatic systems		
C_6H_6	3.7	40.6
$C_{24}H_{12}$	5.8	45.8
$C_{54}H_{18}$	13.2	50.2
graphene	**0.1**	